fluids

MDPI

Article

High-Speed Imaging of Water Hammer Cavitation in Oil–Hydraulic Pipe Flow

Marcus Jansson [1,2,*], Magnus Andersson [1] and Matts Karlsson [1]

[1] Department of Management and Engineering, Linköping University, 58183 Linköping, Sweden; magnus.andersson@liu.se (M.A.); matts.karlsson@liu.se (M.K.)
[2] Underground Rock Excavation, Epiroc Rock Drills AB, 70225 Örebro, Sweden
* Correspondence: marcus.jansson@liu.se

Abstract: A pipe water hammer with column separation was studied in a range of flow rates ($Re = 465$ to 2239) in a test rig with an acrylic glass observation section. Pressure transients were measured with piezoresistive pressure sensors, while the gas evaporation and condensation were captured by high-speed recording with a Photron SA-Z at a frame rate of 75,000 fps. Separation lengths were estimated by a threshold value in the images. The results did not show a sharp gas–oil interface but consisted of small, dispersed bubbles mixed with larger vapor structures, where the bubbles seemed to become smaller after each collapse. These findings differ from the transient cavitating characteristics commonly reported in nonhydraulic piping systems governed by different fluid properties and time scales. Good repeatability, both in terms of pressure transients and bubble distribution, was observed. The column separation was quantified as a metric of separation length, which was consistent between the tests. Combined with pressure measurements, these results may assist in obtaining a better understanding of the transient cavitation dynamics within oil–hydraulic systems as well as be used to improve modelling strategies towards more accurate cavitation erosion predictions.

Keywords: hydraulic transients; column separation; cavitation erosion

check for updates

Citation: Jansson, M.; Andersson, M.; Karlsson, M. High-Speed Imaging of Water Hammer Cavitation in Oil–Hydraulic Pipe Flow. *Fluids* **2022**, 7, 102. https://doi.org/10.3390/fluids7030102

Academic Editor: Kamil Urbanowicz

Received: 21 December 2021
Accepted: 4 March 2022
Published: 9 March 2022

Publisher's Note: MDPI stays neutral with regard to jurisdictional claims in published maps and institutional affiliations.

Copyright: © 2022 by the authors. Licensee MDPI, Basel, Switzerland. This article is an open access article distributed under the terms and conditions of the Creative Commons Attribution (CC BY) license (https://creativecommons.org/licenses/by/4.0/).

1. Introduction

Cavitation erosion is a major concern in most hydraulic applications such as turbines, pumps, and hydraulic percussion units [1]. In the latter case, constant changes in pressure and flow direction will cause water hammer events with possible column separation. Collapsing bubbles cause both pressure waves and high-speed jets which ultimately could induce cavitation erosion. The processes for bubble collapse and cavitation erosion are very short and typically happen on a time scale of microseconds [2]. Repetitive water hammer-induced cavitation may promote erosion in crucial parts of the machinery [3]. Thus, avoiding cavitation or predicting to which extent parts will be subjected to cavitation would increase the lifetime of hydraulic machinery. However, completely removing cavitation might not be possible in all applications, as it may also come with a large cost in terms of reduced performance and efficiency. Accurate estimation of cavitation erosion would aid in the design process of oil–hydraulic components, as well as finding suitable operating conditions, to minimize the more aggressive cavitation events. For example, materials with high cavitation resistance can be used in regions that are more exposed to cavitation erosion. Parts that are subject to severe erosion should be cheap and easy to replace.

Both water hammer and column separation have been extensively studied since the late 19th century when Joukowsky [4] qualitatively described the water hammer phenomenon and derived the famous expression for water hammer surge pressure. A century later, Bergant and Simpson [5] identified two different regimes of column separation: (i) large localized vapor cavities with a large void fraction and (ii) distributed vaporous cavitation with a much lower void fraction. In addition to vaporous cavitation, which

includes column separation, there is also gaseous cavitation [6]. However, the gas release happens at the time scale of seconds and is much slower than vaporous cavitation (microsecond-to-millisecond). Thus, the effects of gas release are expected to be close to negligible during column separation. Further experiments on column separation by Bergant and Simpson [7] showed good repeatability for the main high-pressure peaks, while some high-frequency peaks appeared to be more stochastic. This agreed well with findings from Fan and Tijsseling [8] who studied water hammer cavitation in closed steel tubes. With increased cavitation severity, some high-frequency peaks were less repeatable. In both studies, however, the repeatability was deemed sufficient to study the cavitation regimes on a macro scale. Bergant and Simpson [9] also measured the volume and shape of both discrete cavities and distributed cavitation zones downstream a rapid closing valve. The result showed that the local pressure response from the collapse did not seem to be substantially affected by the shape of the cavitation zone. Thus, pressure measurements alone appear not to be a sufficient metric to assess the vapor distribution in the pipe, nor for the prediction of local cavitation effects.

Prediction of column separation and cavitating pipe flow is typically done by reduced-order models [10–14] or sophisticated computational fluid dynamics (CFD) methods [15–20]. Modelling predictions of column separation cavitation have mainly been validated against measured pressure characteristics (e.g., [3,12,21,22]), while their ability to estimate local cavitation characteristics is still not well understood. Experimental visualization of these flow regimes has been investigated (e.g., [23–27]), however, not at the small time scales associated with oil–hydraulic applications. The shorter time scales could potentially have a large impact on the cavitation behaviour and its erosion effects.

This work aimed to use high-speed imaging and pressure measurements to visualize and characterize column separation oil cavitation within a 0.655 m-long straight acrylic glass pipe at considerably different conditions (fluid properties, pressure levels, and spatiotemporal scales) compared to previous studies within the field. Combined with pressure measurements, these results may assist in achieving a better understanding of the transient cavitation dynamics within oil–hydraulic systems as well as be used for improving modeling strategies toward more accurate cavitation erosion predictions.

2. Materials and Methods

In this section, the test equipment and setup will be briefly explained, including the methods for wave-speed calculation and separation-length estimations. More detailed information on the rig can be found in the previous study by Jansson et al. [3].

2.1. Test Equipment

The test equipment is a modification of that used in previous work by Jansson et al. [3]. The steel pipe was replaced by a pipe in transparent acrylic glass (plexiglass) (Figure 1). To fully monitor the formation of cavitation, the plunger was moved some distance inside the pipe, reducing the effective pipe length to 0.655 m. Pressure sensors were placed at 20 mm, 420 mm, and 620 mm from the contraction. To reduce oil leakage, a polyurethane seal was introduced at the tip of the plunger. The test procedure was very similar, although the pressure level had to be reduced considering the strength of the acrylic glass, which in turn also affected the flow rate. Estimated cavitation numbers G_A [28] from one-dimensional simulations were, however, in the same range as our previous work [3] (Table 1).

The camera used was a Photron FASTCAM SA-Z (https://photron.com/fastcam-sa-z). A similar camera, but with lower throughput, was successfully used in previous studies to observe bubbles in column separation [26]. Two 185 watt LED lights were used to provide continuous background lighting (Figure 1b). The image resolution was 1024 × 256 pixels, and the frame rate was 75,000 fps. All flow rates were shot with a 105 mm lens at a shutter speed of 10 µs. A second set of data was obtained for the highest flow rate, with a 50 mm lens and a shutter speed of 5 µs (Table 2).

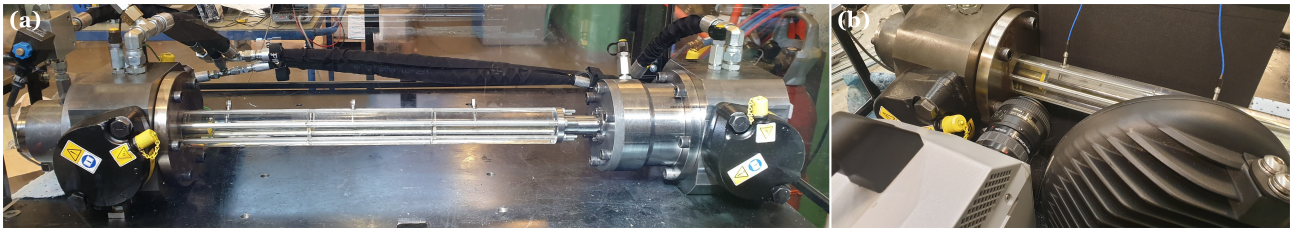


Figure 1. Test setup. (**a**) Overview of the test equipment with acrylic glass observation section. Liquid flows through the pipe from left to right and the plunger is located 80 mm from the upstream end of the pipe. (**b**) Camera setup with a 105 mm lens. One light source was placed close to the observation section while the second light source was further in the background.

Table 1. Estimated cavitation numbers G_A describes the relation between pressure and inertial forces, here represented by the static pressure (p) and the fluid deceleration ($\Delta v/\Delta t$). At lower cavitation numbers (<1), inertial forces are dominating and column separation would be expected.

Orifice	2 mm	3 mm	4 mm	5 mm
p [bar]	21.5	20.9	20.5	19.5
$\Delta v/\Delta t$ [(mm s^{-2})]	0.71	5.10	2.84	3.80
G_A [-]	5.31	2.38	1.27	0.90

Table 2. Flow rate and temperature measurements (given as AVG ± STD) for the different orifice sizes. The Reynolds number (Re) was based on a kinematic viscosity of 4.6×10^{-5} m^2 s^{-1} and inner pipe diameter. At the highest flow rate, two sets of data were obtained with different shutter speed and focal length (denoted low/high).

	Low	Int.	High	High
Orifice size [mm]	2	3	4	5
Flow rate [L min^{-1}]	10.1 ± 0.05	21.7 ± 0.17	35.4 ± 0.21	48.5 ± 0.23
Mean velocity [m s^{-1}]	2.14 ± 0.01	4.60 ± 0.04	7.51 ± 0.04	10.3 ± 0.05
Reynolds number [-]	465	1000	1633	2239
Oil temperature [°C]	33.0 ± 0.30	33.1 ± 1.0	38.7 ± 0.28	40.5 ± 0.13
Image resolution [pixels]	NA	1024 × 256	1024 × 256	1024 × 256
Frame rate [FPS]	NA	75,000	75,000	75,000
Shutter speed [µs]	NA	10	10	5/10
Focal length [mm]	NA	105	105	50/105

2.2. Wave Speed

The wave speed was estimated in different ways. In the pressure measurements, the wave speed could be determined from the time delay between the three measurement points. At low and intermediate flow rates (2–3 mm orifice size), the water hammer was dominating the pressure signal. The wave speed a could thus be derived from the pipe length L and the water hammer frequency f_{wh}, according to

$$a_1 = \frac{4L}{f_{wh}} \tag{1}$$

The wave speed can also be estimated based on the material properties of the system

$$a_2^2 = \frac{1}{\rho\left(\frac{1}{K} + \frac{D\psi}{Ee}\right)} \tag{2}$$

where ρ is the liquid density, K the compressibility modulus of the liquid, D the inner pipe diameter, e the pipe wall thickness, and E the elasticity modulus of the pipe wall [29,30].

Here, ψ is the pipe support factor, which, for a thick-walled pipe anchored upstream, can be estimated as

$$\psi = \frac{2e}{D}(1+\nu)\frac{D}{D+e}(1-\frac{\nu}{2}) \tag{3}$$

where ν is the Poisson's ratio of the pipe material. From Equations (2) and (3) a wave speed of 675 m s^{-1} was derived from the current flow rig data, which was near half compared to the wave speed in the steel pipe counterpart [3]. It is well documented that wave speeds are reduced in plastic pipes compared to steel pipes, and the wave speed can be further reduced in multiphase flows, where the speed is dependent on the amount of nondissolved gases in the liquid [31].

2.3. Column Separation

The pipe surface facing the camera was planar and aligned to the image plane. Furthermore, the refractive indices of plexiglass (1.49) and mineral oil (1.46–1.48) were very similar. Thus, the distortion effects of the pipe were considered to be small compared to the influence of the fluid thickness normal to the image plane. Concerning the latter, the vapor intensity during strong cavitation is expected to be close to homogeneous over the pipe cross-section due to the short time scales of the water hammer (not allowing for gas transportation) and near-even static pressure distribution radially.

Pixel brightness in the ensemble-averaged vapor distribution was used as a proxy for the vapor volume fraction, in a range of $[0, 1]$. All images were subtracted by a vapor-free reference image (before any valve movement) and scaled with respect to the maximum intensity in the image series. Further, a filter was applied to remove low-intensity noise ($<$0.02). Pearson's correlation was used to assess the linear strength between the vapor intensity and fluid thickness in the pipe, and computed during a 3 ms time window (7 time steps) during peak cavitation intensity in the region between the plunger and the first pressure sensor (Figure 2a), corresponding to almost 7000 data points. The Pearson's correlation coefficient was found to be $r = 0.88$ with $p < 0.001$ (Figure 2b), signifying a strong linear monotonic correlation between the parameters. In an attempt to reduce this unwanted effect in the image data, the vapor intensity was, for simplicity, further weighted by a thickness factor $[0, 1]$ over the pipe cross section. To remove pipe boundary effects, 10 pixels were removed from the near-wall region.



Figure 2. (**a**) Nonweighted vapor intensity at 1st peak length ($Re = 2239$). The red box marks the region where the intensity–thickness correlation was evaluated. (**b**) Intensity–thickness scatter plot. Pearson's correlation coefficient $r = 0.88$ ($p < 0.001$). The main deviation between the variables is believed to be associated to the expected flow asymmetry.

From the intensity distribution on the different flow domains (vapor free, severe cavitation), an appropriate vapor cut-off of 0.15 was determined and its sensitivity was investigated ($\pm$0.05). Pixels above the threshold value were considered as vapor and several vapor structures could be observed. To further reduce the effects of fluid thickness and optical distortion in the pipe, the length was estimated for a narrow band (10 pixels) along the pipe centre-line. As expected, separation lengths were dependent on the vapor fraction cut-off and values far from the current threshold would largely over or underestimate the separation from a qualitative point of view. Sensitivity for a 0.05 change in vapor intensity

cut-off can be seen in Figure 3. It is clear that the length estimation is more robust at the early stages while the variation is greatly increased for >10 ms.

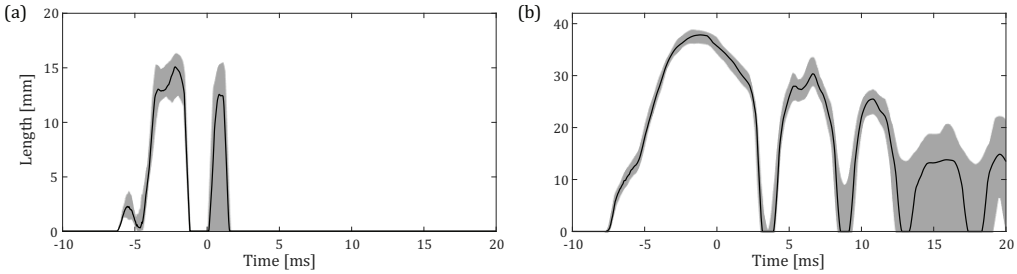


Figure 3. Separation length for 0.15 vapor threshold (black) and ± 0.05 deviation (grey). (**a**) For $Re = 1633$, the length seemed robust for the first separation, while the second separation was highly influenced by the threshold value. (**b**) For $Re = 2239$, the first three separations lengths were not very affected by the threshold value.

3. Results

Flow rates and temperatures for the different set-ups are seen in Table 2. The introduction of the plunger seal reduced the leaking to insignificant levels in comparison to the corresponding steel rig [3]. For the lowest flow rate (Figure 4a), no signs of cavitation could be observed and the pressure was solely governed by a water hammer. At the intermediate flow rate (Figure 4b), the column separation was not very prominent, however, small pressure spikes were visible in addition to the water hammer pressure. At the higher flow rates (Figure 4c,d), the water hammer was clearly disrupted by the column separation, where the 5 mm orifice case promoted clear cavity collapse and liquid column rejoining, evident by the sharp pressure peaks. Noticeably, for the 4 mm case the maximum collapse pressure was lower than the initial pressure, although still very distinct.

For the 5 mm case (Figure 5 and Supplementary Materials), substantial bubbly flow could be observed already before the plunger was completely closed (t1). Vapor bubbles were locally present in the pipe when the recorded (downstream) pressure still was higher than the vapor pressure. At peak cavity length (t2), P1 was inside the cavity and the recorded pressure was well below the vapor pressure. At the moment before the first cavity collapse (t3), a pressure wavefront could be observed in the vapor bubbles. During the high-pressure periods (t4 and t6), no vapor was observed in the pipe. Between the following cavity collapses, vapor bubbles could once again be observed in the pipe (t5). At this instance, small regions of vapor were observed some distance downstream from the main cavity.

For the 4 mm case (Figure 6 and Supplementary Materials), initiation of the vapor cavity (t1) was similar to the 5 mm case. Both the length and duration of the first cavity were visibly shorter. Between the first and second collapse (t5), the bubbles were more spherical and dispersed within the cavitation zone. No real separation of the liquid column could be observed. No bubbles were detected after the second collapse (t6), which is supported by the pressure measurements. No intermediate cavities were observed in any of the cases.

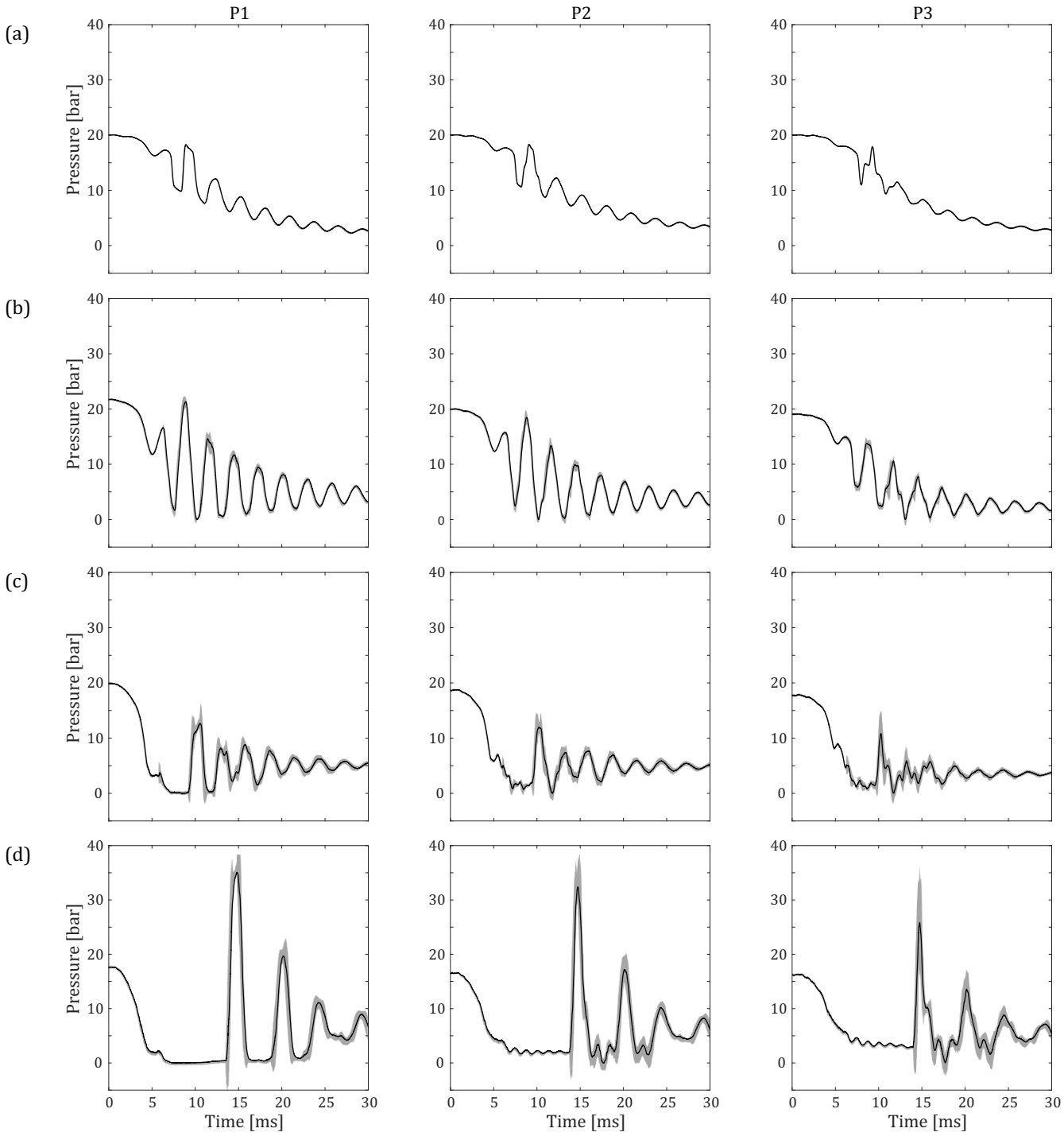


Figure 4. Ensemble-averaged pressure (black) and standard deviation (grey) in the pipe for $N = 10$ tests. Pressure sensors P1, P2, and P3 were located at 20 mm, 220 mm, and 420 mm from the contraction, respectively. Average flow rates corresponds to Reynolds numbers (**a**) $Re = 465$, (**b**) $Re = 1000$, (**c**) $Re = 1633$, and (**d**) $Re = 2239$.

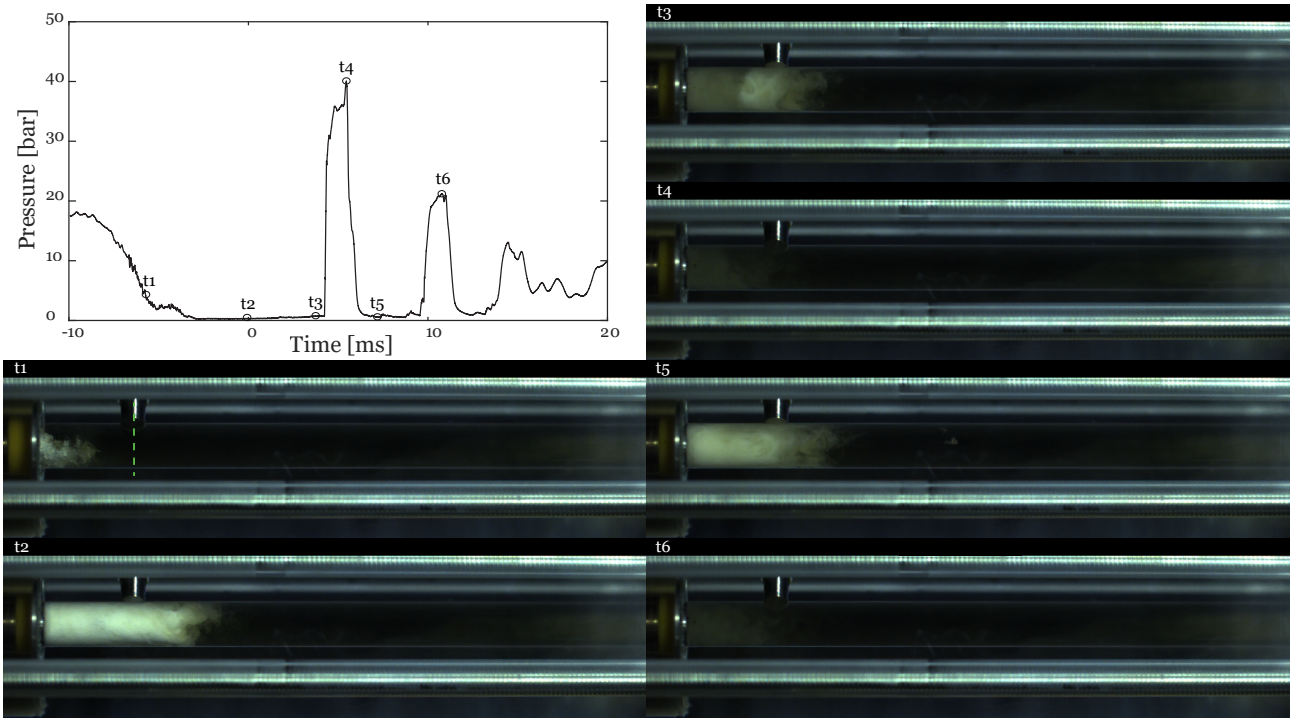


Figure 5. High-speed camera images of the vapor cavities after valve closing for $Re = 2239$ at different snapshots (t1 to t6). The graph inset shows the corresponding pressure response at P1 (green dashed line in t1). For camera settings, see Table 2 (low).

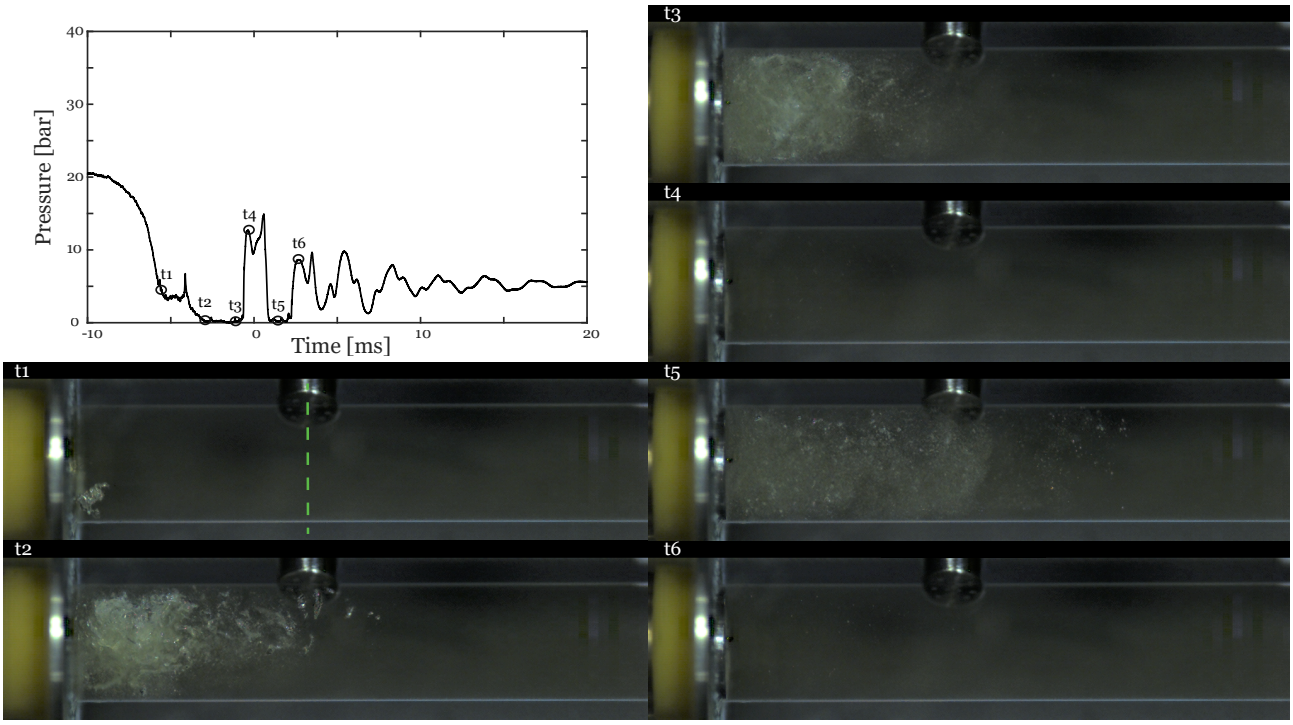


Figure 6. High-speed camera images of the vapor cavities after valve closing for $Re = 1633$ at different snapshots (t1 to t6). The graph inset shows the corresponding pressure response at P1 (green dashed line in t1). For camera settings, see Table 2.

3.1. Wave Speed

The wave speed was measured from the pressure in P1–P3 for all flow cases (Table 3). For the low and intermediate flow rates, the speed was measured from the dominating

frequency according to $f_{wh} = a/4L$. For the high flow rates (4–5 mm orifice), the wave speed was estimated from the time difference and distance between the pressure sensors P1–P3.

Table 3. Wave speeds (in $\mathrm{m\,s^{-1}}$) estimated from the dominating frequency in a power spectral density (PSD) or the time delay (TD) between measurement points.

Orifice Size	2 mm	3 mm	4 mm	5 mm
PSD	920	935	-	-
TD	-	-	1061	946

3.2. Column Separation Length

The column separation length was estimated using the method described in Section 2.3 (Figure 3). For the 5 mm orifice, the separation region was longer in both length and duration compared to the 4 mm orifice. The repeatability was good for both amplitude and timing, especially during the early repetitions when the separation was greater (Figures 7 and 8).

For the 5 mm orifice, the separation length clearly decreased for each iteration and the time between collapses was shorter (Figure 7). The ensemble-averaged vapor distribution was fairly symmetrical, with a slight shift towards the upper part of the pipe. As expected, the recorded pressure peaks correlated well with the timing of the collapse of the vapor structures. For the 4 mm orifice, only a couple of iterations were detectable (Figure 8). The first instance was clearly asymmetrical and originated from the valve throttling. After only a short time (10 ms), the only detectable vapor was small bubbles. The effects from the collapse of these small bubbles were not seen in the average data. However, both bubbles and pressure peaks were more distinct in a single set of data (Figure 6). The estimated maximum separation length for each iteration showed good agreement with the observable vapor regions.

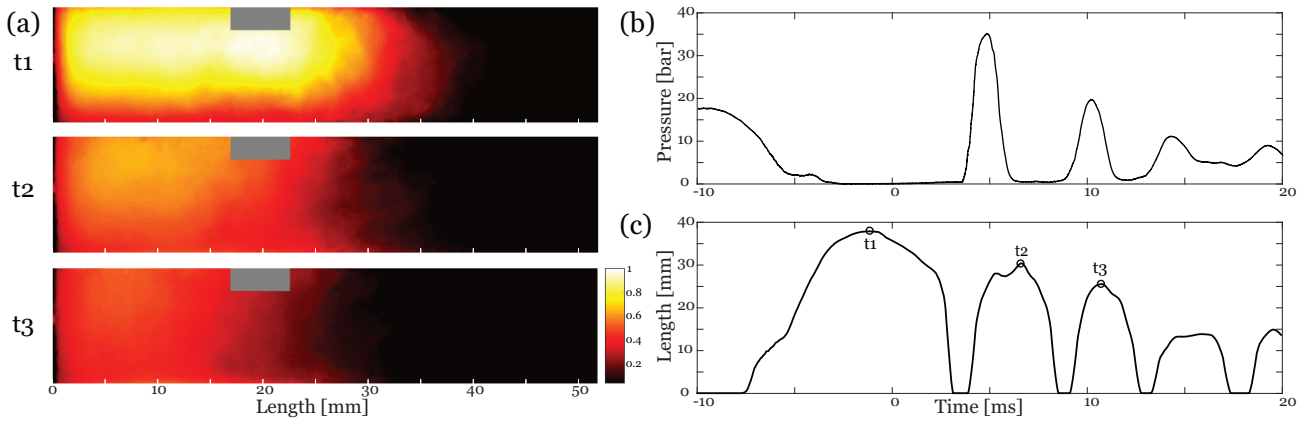


Figure 7. Column separation length for $Re = 2239$. (**a**) Ensemble-averaged vapor distribution for $N = 9$ tests at different snapshots (see t1–t3 in (**c**)). Vapor intensity range $[0.05, 1]$. For camera settings, see Table 2 (high). The region of P1 pressure sensor (grey) has been omitted from the data. (**b**) Ensemble-averaged pressure at P1 pressure sensor. (**c**) Column separation length at 1st to 3rd peak length after valve closing.

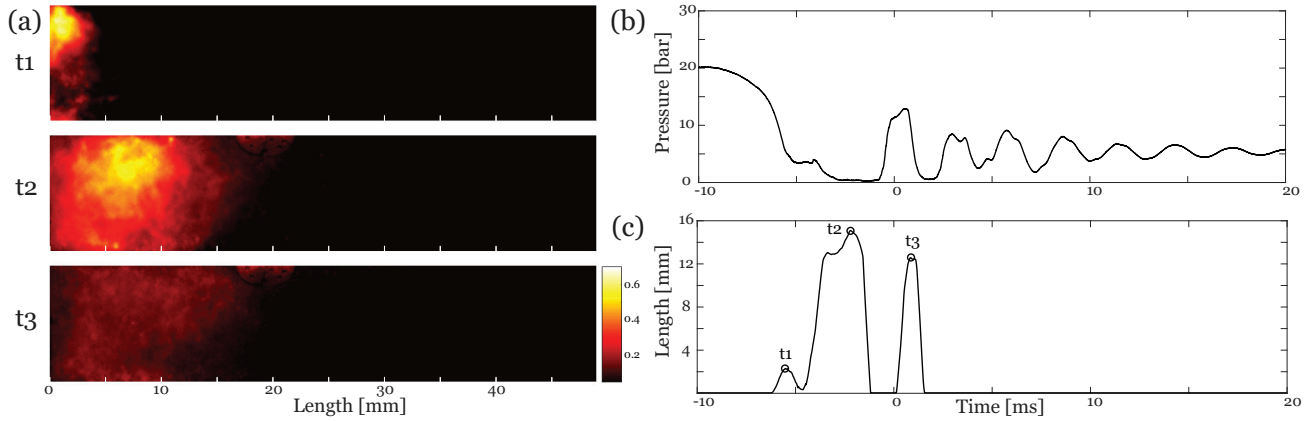


Figure 8. Column separation length for $Re = 1633$. (**a**) Ensemble-averaged vapor distribution for $N = 5$ tests at different snapshots (see t1–t3 in (**c**)). Vapor intensity range $[0.05, 0.7]$. For camera settings, see Table 2. (**b**) Ensemble-averaged pressure at P1 pressure sensor. (**c**) Column separation after valve closing.

3.3. Bubble Dynamics

For the 3 mm orifice, no significant separation was detected in the pressure measurements (Figure 4b). However, spherical bubbles were observed at the tip, or in the vicinity, of the plunger (Figure 9, white arrows). The observed bubbles could be either attached to the plunger or positioned a small distance into the liquid. Most of the attached bubbles were observed close to the pipe wall. Bubbles closer to the center of the plunger were rare, however not completely absent. From the images, it was possible to determine the radius of the bubbles in addition to dR/dT, which quantifies the speed of bubble growth and collapse (Figure 10).

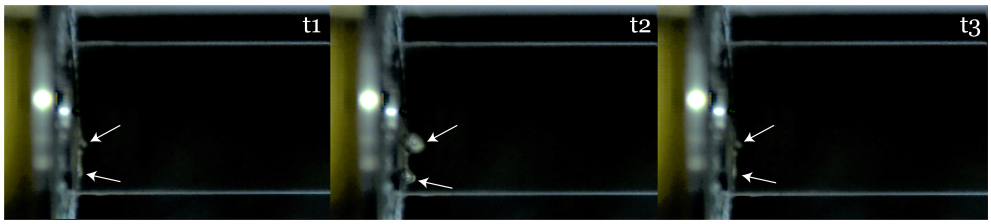


Figure 9. Proximal plunger bubble dynamics for $Re = 1000$, at (**t1**) bubble growth, (**t2**) peak size, and (**t3**) collapse. The bubbles are highlighted with white arrows.

The initial time ($t = 0$) was set to when the bubble was first visible. The growth phase showed a smaller dR/dt than the collapse phase. Bubbles during the initial phase of growth and collapse (C1) lasted for a longer duration than bubbles during the rebound phase (C2). The compression and rebound appeared with the same dR/dt as the initial growth.

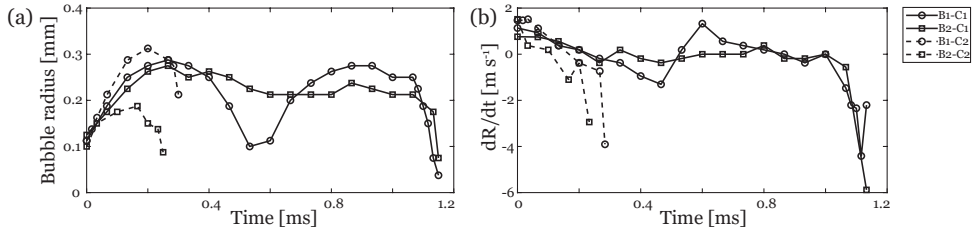


Figure 10. (**a**) Bubble radius. (**b**) Bubble dR/dt. Two bubbles were measured (B1, B2) during initial growth and collapse (C1) and first rebound and collapse (C2).

4. Discussion

The overall characteristics of the pressure response were very similar to our previous study using a steel pipe [3]. The onset of cavitation appeared to be at the intermediate flow rate (Figure 4b) and more prominent at the high flow rates (Figure 4c,d). At the low flow rates (Figure 4a), the water hammer was the only dominant feature. At the intermediate flow rate, the water hammer was still dominant, but small indications of cavitation could be seen in the form of small pressure ripples in addition to the water hammer. The flow rates in the current study were kept lower to ensure the structural integrity of the plexiglass pipe, which explains the lower amplitudes compared to the steel pipe study [3]. It has also been shown by, e.g., Covas et al. [32] that the viscoelastic behaviour of the pipe (retardation) has a large impact on the pressure amplitudes, causing attenuation of the pressure wave and a phase delay in the wave time. Despite the reduced oil pressure and the elasticity of the pipe, the observed cavitation regimes were still similar to our previous experiments using a steel pipe.

The bubble characteristics differ significantly from those observed by Adamkowski et al. [12,22], Bergant and Simpson [9], and Traudt et al. [26], where only a few, large bubbles were observed and clearly gathered in the upper part of the pipe cross-section. Here, the separated part of the liquid column seemed to consist of mainly small, dispersed bubbles contrary to the larger structures typically found in water columns. This could be an effect of the shorter time scales (factor 10^3 lower) since larger structures might not have the time to form. A small vapor asymmetry could however be seen at the highest flow rate (Figure 7), where vapor seemed to gather at the upper part of the pipe. The buoyancy effects were expected to be very small at these short time scales and the asymmetry could possibly come from a nonuniform initial fluid velocity, clearly seen in Figures 5 and 6(t1).

As observed in Figure 5, after the initial closing of the valve, there was no significant convection of the fluid. Cavities seemed to appear at roughly the same regions before each collapse (t3 and t5). Bubbles observed further downstream did not experience displacement in contrast with the studies by, e.g., Traudt et al. [26]. One possible explanation could be the 10-fold difference in time scale. One other main difference is the viscosity of the liquids, where oil has a 40 times higher viscosity than water (0.04 Pa s vs. 0.001 Pa s). It is possible that the initial stages of the separation are similar in both oil and water; however, the temporal resolution of previous studies does not allow us to investigate this any further.

The higher flow rates caused larger separations that lasted for a longer duration. This was expected from previous studies and also supported by the pressure measurements (Figure 4c,d). The length of the bubble region was difficult to measure since it was lacking a sharp interface within the image. Instead, the length was determined using a cut-off threshold similar to what is used in CFD simulations of cavitating flows without interface tracking [33–35]. Although it might be difficult to compare these results to similar studies, this approach is still valid for relative case comparison within this study. It is clear that an increased flow rate caused the bubbles to last for a longer duration. The time between collapses was reduced for each consecutive collapse and thus also the duration of the separation. The length of the bubbly region was also increased, either from increased convection of the bubbles at the initial closing and thus introductions of nucleation sites further down the pipe, and/or due to low pressure at an increased fraction of the pipe. Similar to the duration, the length of the bubbly region was reduced after each collapse.

The image processing in this study was performed to reduce uncertainties from the experimental setup. However, the postprocessing relies on various assumptions that will attenuate or amplify the sources of errors differently within each image and across the image set. Nevertheless, we do not believe that these effects are sufficient enough to jeopardize the general findings and conclusions of this study. The thickness weighting of the vapor intensity is not believed to have any noticeable effect on the separation length, since the length is measured close to the pipe centre. For the highest flow rate, where the vapor distribution is close to homogeneous over the pipe cross section, the vapor intensity

at the pipe centre would be sufficient to describe the separation region. However, it is not as obvious that this approximation works equally well at the lower flow rate. Nevertheless, the estimated length seemed to agree well with the observable vapor (Figure 8).

The short time scale influenced the effects of the dissolved gases. During evaporation, it could be expected that some dissolved gases would come out of the solution and enter the vapor cavities. This process is however much slower than that of evaporation/condensation and it is not well known how big this effect would be. During condensation, much of this gas will not be able to dissolve into the liquid and thus form small bubbles instead. These microbubbles would serve as nucleation sites during successive cavitation events. Traudt et al. [26] hypothesized that this could explain why bubbles were observed to decrease in size but increase in numbers. Indeed, in the present study, this phenomenon could be observed at the higher flow rates (Figures 5 and 6).

The bubble dynamics for more spherical bubbles could be observed in Figure 10. All bubbles showed a similar growth rate during both the initial growth and the rebound phase. As expected, the growth rate seemed to decrease with an increased bubble radius. The final bubble collapse appeared at a higher rate than the bubble growth.

5. Conclusions

The oil–hydraulic column separation observed in our previous study using a steel pipe [3] was confirmed by reproducing the experiments with a transparent pipe made of acrylic glass. The column separation dynamics were captured by high-speed imaging with a Photron SA-Z camera. The observed separation did not have a clear interface but consisted of small dispersed bubbles mixed with larger vapor structures, where the bubbles seemed to become smaller after each successive collapse; findings which differ from the transient cavitating characteristics commonly reported in nonhydraulic piping systems governed by different fluid properties and time scales. The experiments showed very good repeatability, both in terms of pressure transients and the appearance of vapor cavities. Although these results would add to the understanding of the cavitation characteristics, good methods of quantification are still needed to use such data for cavitation erosion prediction models within oil–hydraulic applications.

Supplementary Materials: The following are available online at https://www.mdpi.com/article/10.3390/fluids7030102/s1, Video S1: Column separation at $Re = 1633$ and $Re = 2239$.

Author Contributions: Conceptualization, M.J., M.A. and M.K.; methodology, M.J., M.A. and M.K.; formal analysis, M.J.; investigation, M.J.; writing—original draft preparation, M.J.; writing—review and editing, M.J. and M.A.; visualization, M.J.; supervision, M.A. and M.K. All authors have read and agreed to the published version of the manuscript.

Funding: This research was funded by Epiroc Rock Drills AB.

Data Availability Statement: Some representative data from this study are openly available in FigShare at https://doi.org/10.6084/m9.figshare.17262641, retrieved 8 March 2022. The complete data presented in this study are available on request from the corresponding author.

Conflicts of Interest: M.J. is an employee at Epiroc Rock Drills AB. The authors declare no other conflict of interest.

References

1. Li, S. *Cavitation of Hydraulic Machinery*; World Scientific: Singapore, 2000; Volume 1.
2. Dular, M.; Požar, T.; Zevnik, J. High speed observation of damage created by a collapse of a single cavitation bubble. *Wear* **2018**, *418*, 13–23. [CrossRef]
3. Jansson, M.; Andersson, M.; Pettersson, M.; Karlsson, M. Experimental Assessment of Water Hammer-Induced Column Separation in Oil-Hydraulic Pipe Flow. *J. Fluids Eng.* **2019**, *141*, 101107. [CrossRef]
4. Joukowsky, N. *Über den Hydraulischen Stoss in Wasserleitungsrohren*; Académie Impériale des Sciences: St. Petersbourg, Russia, 1900.
5. Bergant, A.; Simpson, A. Pipeline Column Separation Flow Regimes. *J. Hydraul. Eng.* **1999**, *125*, 835–848. [CrossRef]
6. Bergant, A.; Simpson, A.R.; Tijsseling, A.S. Water hammer with column separation: A historical review. *J. Fluids Struct.* **2006**, *22*, 135–171. [CrossRef]

7. Simpson, A.; Bergant, A. Interesting lessons from column separation experiments. In Proceedings of the 7th International Conference on Pressure Surges and Fluid Transients in Pipelines and Open Channels, Harrogate, UK, 16–18 April 1996; pp. 83–97.
8. Fan, D.; Tijsseling, A. Fluid-Structure Interaction with Cavitation in Transient Pipe Flows. *J. Fluids-Eng.-Trans. Asme-J. FLUID ENG* **1992**, *114*, 268–274. [CrossRef]
9. Bergant, A.; Simpson, A. Visualisation of transient cavitating flow in piping systems. *J. Mech. Eng.* **1996**, *42*, 1–16.
10. Streeter, V.L. Transient Cavitating Pipe Flow. *J. Hydraul. Eng.* **1983**, *109*, 1407–1423. [CrossRef]
11. Simpson, A.R.; Bergant, A. Numerical Comparison of Pipe-Column-Separation Models. *J. Hydraul. Eng.* **1994**, *120*, 361–377. [CrossRef]
12. Adamkowski, A.; Lewandowski, M. A new method for numerical prediction of liquid column separation accompanying hydraulic transients in pipelines. *J. Fluids Eng.* **2009**, *131*, 071302. [CrossRef]
13. Urbanowicz, K.; Firkowski, M. Extended Bubble Cavitation Model to predict water hammer in viscoelastic pipelines. *J. Phys. Conf. Ser.* **2018**, *1101*, 012046. [CrossRef]
14. Yang, J.; Yang, J.; Guo, W.; Luo, J.; Fu, G. Investigation of water column separation induced by pressure pulsation based on critical cavitation rate model. *IOP Conf. Ser. Earth Environ. Sci.* **2021**, *774*, 012055. [CrossRef]
15. Patella, R.F.; Archer, A.; Flageul, C. Numerical and experimental investigations on cavitation erosion. *IOP Conf. Ser. Earth Environ. Sci.* **2012**, *15*, 022013. [CrossRef]
16. Li, Z.; Pourquie, M.; Terwisga, T. Assessment of Cavitation Erosion With a URANS Method. *J. Fluids Eng.* **2014**, *136*, 041101. [CrossRef]
17. Pinho, J.; Lema, M.; Rambaud, P.; Steelant, J. Multiphase Investigation of Water Hammer Phenomenon Using the Full Cavitation Model. *J. Propuls. Power* **2014**, *30*, 105–113. [CrossRef]
18. Wang, H.; Zhou, L.; Liu, D.; Karney, B.; Wang, P.; Xia, L.; Ma, J.; Xu, C. CFD Approach for Column Separation in Water Pipelines. *J. Hydraul. Eng.* **2016**, *142*, 04016036. [CrossRef]
19. Gao, H.; Tang, X.; Li, X.; Shi, X. Analyses of 2D transient models for vaporous cavitating flows in reservoir-pipeline-valve systems. *J. Hydroinformatics* **2018**, *20*, 934–945. [CrossRef]
20. Tang, X.; Duan, X.; Gao, H.; Li, X.; Shi, X. CFD Investigations of Transient Cavitation Flows in Pipeline Based on Weakly-Compressible Model. *Water* **2020**, *12*, 448. [CrossRef]
21. Warda, H.A.; Wahba, E.M.; El-Din, M.S. Computational Fluid Dynamics (CFD) simulation of liquid column separation in pipe transients. *Alex. Eng. J.* **2020**. [CrossRef]
22. Adamkowski, A.; Lewandowski, M. Investigation of hydraulic transients in a pipeline with column separation. *J. Hydraul. Eng.* **2012**, *138*, 935–944. [CrossRef]
23. Bunt, E. Preliminary study of valve cavitation in pipelines. *J. S. Afr. Inst. Mech. Eng.* **1953**, *2*, 235–260.
24. Blind, H. Nichtstationäre Strömungen in Unterwasserstollen. In *Veröffentlichungen zur Erforschung der Druckstoßprobleme in Wasserkraftanlagen und Rohrleitungen*; Springer: Berlin/Heidelberg, Germany, 1956; pp. 67–108.
25. Escande, L.; Nougaro, J. Etude théorique et expérimentale du fonctionnement en charge des canaux de fuite en l'absence de cheminée d'équilibre. *La Houille Blanche* **1953**, 607–639. http://dx.doi.org/10.1051/lhb/1953053. [CrossRef]
26. Traudt, T.; Bombardieri, C.; Manfletti, C. High Speed Imaging of Water Hammer with Column Separation, BHR Group. In Proceedings of the 12th International Conference on Pressure Surges, Dublin, Ireland, 18–20 November 2015; pp. 47–57, ISBN 9781-85598-151-5-11.5-12.
27. Kojima, E.; Shinada, M.; Shindo, K. Fluid Transient Phenomena Accompanied with Column Separation in Fluid Power Pipeline: 1st Report, On the Horizontal Pipeline Downstream of a Valve Instantaneously Closed. *Bull. JSME* **1984**, *27*, 2421–2429. [CrossRef]
28. Fatjo, G.G.A. New Dimensionless Number To Predict Cavitation In Accelerated Fluid. *Int. J. Comput. Methods Exp. Meas.* **2016**, *4*, 484–492. [CrossRef]
29. Wylie, E.B.; Streeter, V.L. *Fluid Transients*; McGraw-Hill International Book Co.: New York, NY, USA, 1978; 401p.
30. Watters, G.Z. *Analysis and Control of Unsteady Flow in Pipelines*; Butterworths: Boston, MA, USA, 1984.
31. Jonkobilov, U.; Jonkobilov, S.; Bekjonov, R.; Norchayev, A. Shock wave velocity in two-phase pressure flow. *IOP Conf. Ser. Mater. Sci. Eng.* **2021**, *1030*, 012129. [CrossRef]
32. Covas, D.; Stoianov, I.; Ramos, H.; Graham, N.; Maksimovic, C. The dynamic effect of pipe-wall viscoelasticity in hydraulic transients. Part I—Experimental analysis and creep characterization. *J. Hydraul. Res.* **2004**, *42*, 517–532. [CrossRef]
33. Ait Bouziad, Y.; Farhat, M.; Guennoun, F.; Kueny, J.L.; Avellan, F.; Miyagawa, K. Physical Modelling and Simulation of Leading Edge Cavitation, Application to an Industrial Inducer. In Proceedings of the Fifth International Symposium on Cavitation (CAV2003), Osaka, Japan, 4 November 2003.

34. Vaz, G.; Hally, D.; Huuva, T.; Bulten, N.; Muller, P.; Becchi, P.; Herrer, J.; Whitworth, S.; Macé, R.; Korsström, A. Cavitating Flow Calculations for the E779A Propeller in Open Water and Behind Conditions: Code Comparison and Solution Validation. In Proceedings of the Fourth International Symposium on Marine Propulsors (Smp'15), Austin, TX, USA, 31 May–4 June 2015.
35. Huan, Y.y.; Liu, Y.y.; Li, X.j.; Zhu, Z.c.; Qu, J.t.; Zhe, L.; Han, A.d. Experimental and numerical investigations of cavitation evolution in a high-speed centrifugal pump with inducer. *J. Hydrodyn.* **2021**, *33*, 140–149. [CrossRef]